Intense-field photodissociation of H_2^+: Comparison of time-dependent and time-independent calculations

Robert W. Heather and Frederick H. Mies
National Institute of Standards and Technology, Gaithersburg, Maryland 20899
(Received 8 July 1991)

The decay of the initial bound-state population and the fragment kinetic-energy distribution produced by the intense-field photodissociation of H_2^+ are calculated using both a time-dependent and a time-independent method. The time-dependent method calculates the time evolution of the wave function describing H_2^+ interacting with a classical time-dependent laser field by repeated application of a short-time propagator. The time-independent method constructs a wave packet using the energy eigenstates of the total molecule-plus-field Hamiltonian with the field expressed as a superposition of quantized photon number states. Specifically, the wave packet represents an initial bound-state wave function of the field-free molecule subjected to a coherent photon state that simulates the classical radiation field at $t=0$. The subsequent decay of this nonstationary state can be viewed as a laser-induced predissociation of field-dressed bound states into field-dressed continuum states with various numbers of photons absorbed from the field. For very rapid dissociation, the decays of the initial bound-state population calculated by both methods are in good agreement if a square pulse shape is used and the initial phase of the time-dependent interaction is averaged over. The fragment kinetic-energy distributions calculated by the two methods are in good agreement if they are compared at times when there is unit probability for dissociation. For slow to moderately rapid dissociation, averaging over the initial phase of the field is unnecessary because there is no rapid decay component. However, this also implies that the wave function must be propagated over many time steps before complete dissociation is achieved. To avoid this, we describe a procedure for fitting a short-time line-shape function, which represents incomplete dissociation of the initial state, to the nondepletion-limit fragment kinetic-energy distribution. A parametric fit to the calculated distributions allows us to extract very accurate estimates of decay rates, ac Stark shifts, and branching ratios.

PACS number(s): 42.60.−v

I. INTRODUCTION

Developments in laser technology have made it possible to study photon-matter interactions over many orders of magnitude in the electric field intensity. This range of intensities extends from where the interaction is a weak perturbation to where the field strength is comparable to or greater than the atomic field. At high intensities one sees interesting phenomena such as above-threshold ionization of atoms [1] and above-threshold dissociation of molecules [2–5], in which photons are absorbed in the continuum.

It is not surprising that the applicability of various theoretical methods for studying photon-matter interactions depends on the strength of the interaction. For example, perturbation theory works well at low intensity, i.e., when the magnitude of the interaction is less than the intrinsic atomic or molecular frequencies [6]. At higher intensities nonperturbative methods are preferable. One such method, presented in the preceding paper [7], is based on constructing wave packets using the solutions of time-independent scattering theory with a time-independent radiation field expanded in quantized photon number states. An initial bound-state wave packet is expanded in a set of such dressed (atom-plus-field or molecule-plus-field) scattering states, and the process becomes one of laser-induced autoionization or predissociation of bound dressed states into different ionization or dissociation continua, one for each absorbed or emitted photon [7–10]. The coupled equations arising from the wave-function expansion can be solved using techniques commonly used in multichannel scattering theory. The computational effort increases with increasing strength of the interaction, because the number of coupled equations one must solve is equal to the number of atom-plus-field or molecule-plus-field basis functions in the wave-function expansion, which increases with increasing intensity and wavelength.

Another class of nonperturbative methods involves solving the time-dependent Schrödinger equation in the interaction picture and calculates the time evolution of the wave function describing the atom or molecule interacting with the time-dependent laser field [11–16]. From the wave function one can calculate such quantities as the ionization or dissociation probability as a function of time and the kinetic-energy distribution of the photoelectrons or photofragments. The computational effort is proportional to the number of time steps, which is proportional to the time it takes the atom or molecule to ionize or dissociate. Unlike the time-independent method just described, the computational effort associated with time-dependent methods may actually decrease with increasing intensity, assuming that additional electronic states are not populated, since the ionization or dissocia-

tion rate generally increases with intensity. At low intensities, however, the propagation time may be prohibitively long unless one uses short pulses.

The time-dependent theory of intense-field photodissociation usually assumes a classical molecule-field interaction of the form $\mu(R)f(t)\cos(\omega t)$, where $\mu(R)$ is a dipole or transition dipole function which varies with the fragment separation R, and $f(t)\cos(\omega t)$ describes the time variation of the electric field. At $t=0$ the molecule initially is in a field-free eigenstate, and the laser-pulse-shape function $f(t)$ determines how the radiative interaction is turned on and off. The wave function is propagated in time until $f(t)=0$, which implies that the laser pulse has left the vicinity of the molecule, or when the expectation value of $\mu(R)$ vanishes. It is important to note that with the time-dependent theory one is free to choose the functional form of $f(t)$, e.g., to study pulsed excitation.

Actually, the time-independent theory can be derived in several ways. In the Floquet ansatz [10] one continues to use a classical expression, e.g., $\mu(R)E^0\cos(\omega t)$, for the molecule-field interaction, and takes advantage of the periodicity to expand the time dependence of the wave function in a Fourier series. Upon expressing the $\cos(\omega t)$ as a sum of exponentials and integrating over an optical cycle, one obtains a set of time-independent coupled equations in which states with Fourier index n are coupled to states with $n\pm1$, corresponding to absorption or emission of a photon, and the molecule-field coupling is the same in each Floquet block.

One also can describe the molecule-field interaction quantum mechanically [7–9] by expanding the total wave function in photon number states $|N-n\rangle$ which are eigenstates of the radiation-field Hamiltonian, where we define $n=0,\pm1,\pm2,\ldots$ as a photon channel index that labels each block. The coupled equations resulting from the wave-function expansion are blocked similar to those in the Floquet theory except that the molecule-field interaction is proportional to $(N-n)^{1/2}\approx N^{1/2}$. The fragment kinetic-energy distribution is calculated by projecting the wave function describing the initial state of the molecule onto the solutions of the coupled equations as a function of energy [7].

If a quantum-mechanical description of the molecule-field interaction is used, the initial-state wave function must be a product of a wave function describing the molecule and a wave function describing the initial state of the field. One can make contact with the time-dependent theory, which uses a classical description of the field, i.e., $E^0\cos(\omega t)$, by expressing the wave function describing the field as a coherent superposition of photon number states, such that the expectation value of the electric field operator in this state is equal to the classical value [17]. It has been shown [7] that for most practical applications it is entirely adequate to simply represent the field by some average number state $|\overline{N}\rangle$, even though in this case the expectation value of the electric field operator is actually zero instead of $E^0\cos(\omega t)$ because the phase is completely uncertain.

An important difference between the time-independent and time-dependent descriptions of the process is that the former is a steady state description in which the molecule is always interacting with the field; whereas in the latter descriptions the molecule interacts with the field only when $f(t)\neq0$. This difference is important when discussing issues of initial-state preparation.

In principle the time-independent (wave-packet) methods and the time-dependent methods should yield essentially equivalent results, although in practice they are somewhat complementary in that the first one works best in the limit of weak fields and the second in the limit of strong fields. This complementarity is made manifest in a computational sense: the computational effort for time-independent methods decreases with decreasing field intensity, because fewer molecule-plus-field basis functions are needed in the wave-function expansion, whereas time-dependent methods uncover the computational effort of the decreases with increasing intensity, because the molecule dissociates more rapidly and the wave function is propagated for fewer time steps. This raises the question of whether there exists a middle ground where both methods are equally applicable. In this paper we explore this question by using both methods to calculate the decay of the initial bound-state population and the fragment kinetic-energy distribution produced by the intense-field photodissociation of H_2^+, using several intensities, wavelengths, and initial vibrational states. Of primary interest is how sensitive the results are to the basic assumptions that are required to derive the time-independent theory from the time-dependent theory, e.g., assuming a square pulse shape or averaging the interaction over the optical cycle. We note that H_2^+ photodissociation has attracted both experimental and theoretical interest, and that peaks in the fragment kinetic-energy distribution, due to above-threshold dissociation (ATD), have been observed experimentally [2–5] and in theoretical calculations [8,15].

In addition to ATD, another interesting feature of intense-field photodissociation is laser-induced bond softening [5], in which the molecular bond is weakened due to the molecule-field interaction. This phenomenon can be easily understood upon inspection of the dressed-state potential energy curves of the time-independent theory: increasing the molecule-field interaction increases the separation of the adiabatic potentials at the avoided crossing of the diabatic dressed-state potentials, which has the effect of lowering both the barrier to dissociation and the vibrational force constant if the curve crossing occurs at an internuclear separation greater than the equilibrium separation.

Peaks in the experimental photoelectron kinetic-energy distribution [4,5,18] suggest that a distribution of H_2^+ vibrational states is populated by the intense-field ionization of H_2. Bond softening affects the higher vibrational states the most, since the initial-state field-free vibrational wave function is projected onto more field-dressed vibrational states, and possibly continuum states if the barrier to dissociation is pulled down far enough. This rapidly dissociating continuum component is treated differently in the time-independent and time-dependent theories, because the time-independent theory assumes that dissociation is much slower than the optical period in order to justify averaging over the optical cycle. In the time-

dependent method, how the continuum component appears in the kinetic-energy distribution is sensitive to the pulse shape, i.e., on how rapidly the interaction is turned on. Rapidly turning on the interaction with a square pulse shape, the Fourier transform of which is not monochromatic for finite pulse widths, will cause transients to appear in the kinetic-energy distribution if dissociation or ionization is rapid, which is the case for the continuum component.

This paper is organized as follows. In Sec. II the two-state model of H_2^+ is described. This model previously has been used to study ATD using both time-dependent [15] and time-independent [8] methods. In Sec. III the time-dependent and time-independent methods are presented, along with a method for obtaining depletion-limit quantities at short times. In Sec. IV the fragment kinetic-energy distributions and the decay of the initial-state population, calculated using both methods, are compared for several wavelengths, intensities, and initial vibrational states.

II. H_2^+ MODEL SYSTEM

H_2^+ is the simplest molecule and its electronic structure has been studied extensively. Our model includes only two electronic states: the bound $^2\Sigma_g^+$ and the unbound $^2\Sigma_u^+$ states [$(1s)\sigma_g$ and $(2p)\sigma_u$ in the united-atom limit], which are asymptotically degenerate and correlate to symmetric and antisymmetric combinations of atomic $1s$ states [19]. The $^2\Sigma_g^+$ and $^2\Sigma_u^+$ electronic states are described by the wave functions $\phi_g(\mathbf{r},R)$ and $\phi_u(\mathbf{r},R)$, respectively, which are eigenfunctions of the electronic Hamiltonian $H_{\rm el}(\mathbf{r},R)$, where $\mathbf{r}$ is the electron coordinate and R is the nuclear separation.

Nuclear motion is influenced by the Born-Oppenheimer potential energy curves (here taken to be attractive and repulsive Morse potential functions [10])

$$V_g(R)=\int d\mathbf{r}\,\phi_g(\mathbf{r},R)^* H_{\rm el}(\mathbf{r},R)\phi_g(\mathbf{r},R) \tag{1}$$

$$=D[Y(R)^2-2Y(R)] \tag{2}$$

and

$$V_u(R)=\int d\mathbf{r}\,\phi_u(\mathbf{r},R)^* H_{\rm el}(\mathbf{r},R)\phi_u(\mathbf{r},R) \tag{3}$$

$$=D[Y(R)^2+2.22Y(R)]\ , \tag{4}$$

in atomic units, where $Y(R)=\exp[-\alpha(R-R_0)]$, $D=0.102\,62$ a.u., $\alpha=0.72a_0^{-1}$, and $R_0=2.0a_0$.

Nuclear motion in the $^2\Sigma_g^+$ and $^2\Sigma_u^+$ states is coupled by the molecule-field interaction:

$$V_{gu}(R,t)=\frac{-e}{mc}\,\mathbf{A}(\mathbf{r}=0,t)\cdot\int d\mathbf{r}\,\phi_g(\mathbf{r},R)^*\mathbf{p}\phi_u(\mathbf{r},R)\ , \tag{5}$$

here expressed in the radiation-field (velocity) gauge and the dipole approximation, where $\mathbf{A}(\mathbf{r}=0,t)$ is the vector potential and $\mathbf{p}$ is the electron momentum operator. Assuming that $\mathbf{A}(\mathbf{R}=0,t)=c\mathbf{E}^0\sin(\omega t)/\omega$, then Eq. (5) can be recast as [20]

$$V_{gu}(R,t)=\mu_{gu}(R)E^0\cos(\omega t)[V_u(R)-V_g(R)]/\hbar\omega\ , \tag{6}$$

where E^0 is the maximum amplitude of the electric field vector, with a unit polarization vector $\hat{\mathbf{e}}$ which defines the transition dipole matrix element

$$\mu_{gu}(R)=e\int d\mathbf{r}\,\phi_g(\mathbf{r},R)^*\mathbf{r}\cdot\hat{\mathbf{e}}\phi_u(\mathbf{r},R)\ . \tag{7}$$

This is taken to be of the form

$$\mu_{gu}(R)=(\hat{\mathbf{R}}\cdot\hat{\mathbf{e}})(1.07+7.2\{\exp[0.55(R-R_0)]-1\}) \tag{8}$$

(in atomic units) where $\hat{\mathbf{R}}$ is a unit vector defined by the internuclear coordinate $\mathbf{R}$. We use the radiation-field gauge because, unlike the electric field gauge, the molecule-field interaction in Eq. (6) vanishes at large R due to the $V_u(R)-V_g(R)$ term, which goes to zero. This makes it possible to apply the proper asymptotic analysis of the wave function.

Note that gauge invariance can be assured only if a complete set of electronic states ϕ_Λ is included in the wave-function expansion [21]. In our model we include only the $\Lambda=g$ ($^2\Sigma_g^+$) and $\Lambda=u$ ($^2\Sigma_u^+$) electronic states. As discussed elsewhere [7], this causes great sensitivity to the choice of gauge, and brings into question the accuracy of the results presented in this paper. However, since our purpose here is to demonstrate the excellent agreement one obtains between the time-dependent and time-independent methods of calculation, we ask the reader to accept the limitations imposed by the two-electronic-state approximation. Further details of these calculations are given in the preceding paper [7].

In fact, the model is simplified even further by severely restricting the rotational basis used in the expansion of the total wave function. In principle, we should introduce a complete set of rotational states $Y_{J,M}(\hat{\mathbf{R}})$ in order to span the space associated with the molecular orientation vector $\hat{\mathbf{R}}$. Normally this would be accomplished by expanding the total wave function over a complete set of electronic-rotational channel states $\psi_\gamma(\mathbf{x},R)=\phi_\Lambda(\mathbf{r},R)Y_{J,M}(\hat{\mathbf{R}})$ which together span the entire space of the vector $\mathbf{x}=\mathbf{r},\hat{\mathbf{R}}$. Instead, we choose to ignore many interesting optical pumping and orientation effects associated with the rotational state of H_2^+ and expand the total wave function with only a single pair of electronic-rotational channel states represented simply as $\psi_g(\mathbf{x},R)=\phi_g Y_{J,M}$ and $\psi_u(\mathbf{x},R)=\phi_u Y_{J',M'}$, respectively, first in the time-dependent expression, Eq. (10), and later in the time-independent expansion, Eq. (24). In this model we introduce a mean rotational quantum number J and merely add a common centrifugal potential $\hbar^2J(J+1)/m_HR^2$ to each of the potentials V_g and V_u in Eqs. (1) and (3), respectively. The unit vector in Eq. (8) should now be replaced by the rotational line strength $S_{JJ'}=\langle Y_{J,M}|\hat{\mathbf{R}}\cdot\hat{\mathbf{e}}|Y_{J',M'}\rangle$. Depending on how one chooses to interpret the product of rotational line strength and electric field, $S_{JJ'}E^0=S_{JJ'}(8\pi I/c)^{1/2}$, which now appears in Eq. (6), where I is the laser intensity, we can qualitatively model several experimental situations. In particular, the high degree of fragment orientation seen experimentally for linear polarization [4,5] suggests that we might want to take $S_{JJ'}\approx 1$ to simulate $\hat{\mathbf{R}}\cdot\hat{\mathbf{e}}\approx 1$ alignment of the molecule in the laser field. Current studies, which include a more complete expansion in ro-

tational channel states, are in progress to test this model and achieve a more quantitative comparison with experiment. Thus we must stress that we are presenting a model system designed to facilitate the comparison of the time-dependent and time-independent methods to each other, rather than to experiment.

III. THEORY

A. Time-dependent method

In the time-dependent method used in this study, the wave function describing the system is propagated in time by the repeated operation of a short-time propagator $U(t_{j+1},t_j)$, i.e.,

$$\Psi(t=N\Delta t,\mathbf{x},R)=\left[\prod_{j=0}^{N-1}U(t_{j+1},t_j)\right]\Psi(t=0,\mathbf{x},R)\ , \quad (9)$$

where $t_{j+1}=t_j+\Delta t$.

The total wave function is expanded in eigenstates of the electronic Hamiltonian and scattering wave functions:

$$\Psi(t,\mathbf{x},R)=\psi_g(\mathbf{x},R)G_g(t,R)+\psi_u(\mathbf{x},R)G_u(t,R)\ , \quad (10)$$

where $G_g(t,R)$ and $G_u(t,R)$ are wave functions describing nuclear motion associated with the ψ_g and ψ_u channel states, respectively. Substituting Eq. (10) into the time-dependent Schrödinger equation, operating from the left with $\psi_g(\mathbf{x},R)$ and $\psi_u(\mathbf{x},R)$, and integrating over $\mathbf{x}$, one obtains an expression for the time evolution of $G_g(t,R)$ and $G_u(t,R)$ (in matrix form):

$$i\hbar\frac{\partial\underline{G}(t,R)}{\partial t}=[\underline{T}_R+\underline{V}(t,R)]\underline{G}(t,R)\ , \quad (11)$$

where $\underline{T}_R=\underline{I}T_R$ is the kinetic-energy operator for the relative motion of the nuclei, $\underline{I}$ is a 2×2 unit matrix,

$$\underline{V}(t,R)=\begin{bmatrix}V_g(R) & V_{gu}(t,R)\\ V_{gu}(t,R) & V_u(R)\end{bmatrix} \quad (12)$$

is the potential matrix, and

$$\underline{G}(t,R)=\begin{bmatrix}G_g(t,R)\\ G_u(t,R)\end{bmatrix} \quad (13)$$

is a column vector containing the nuclear components of the wave function.

Equation (11) permits us to write the short-time propagator in "split operator" form [22],

$$\underline{U}(t_{j+1},t_j)=\exp\left[-\frac{i\Delta t}{2\hbar}\underline{T}_R\right]\exp[-i\underline{V}'(t_j,R)\Delta t/\hbar]\times\exp\left[-\frac{i\Delta t}{2\hbar}\underline{T}_R\right]\ , \quad (14)$$

where

$$\underline{V}'(t_j,R)=\int_{t_j}^{t_{j+1}}dt\ \underline{V}(t,R)/\Delta t \quad (15)$$

is the interaction averaged over the time step.

In practice $\underline{G}(t=0,R)$ is evaluated on a position grid $\{R_j\}$, $j=1,2,\ldots,M$, which is related to the wave function evaluated on a momentum grid $\{p_k\}$, $k=1,2,\ldots,M$, by a discrete Fourier transform. When applying $\underline{U}(t_{j+1},t_j)$ to the wave function, it is best to calculate the operation of the kinetic-energy part of the propagator on the wave function in the momentum representation, and the operation of the potential energy part of the propagator on the wave function in the position representation. In each time step one must also transform the wave function to a representation that diagonalizes $\underline{V}(t,R)$ [15,23].

One problem associated with calculating the time evolution of a wave function corresponding to an unbound degree of freedom is that it becomes spatially extended at long times. To deal with this problem we often use a procedure described in Ref. [15], which splits the wave function during its evolution into an interaction region piece (where $\partial\underline{V}/\partial R\neq0$) and asymptotic region pieces (where $\partial\underline{V}/\partial R\approx0$). We can then propagate the interaction region piece using the short-time propagator, Eq. (14), and the asymptotic region pieces using a (long-time) free-particle propagator. Details of the time-dependent propagation and the wave-function splitting procedure, for this particular H_2^+ system, are given in Ref. [15]. It might be appropriate to mention at this point that the present calculations using the velocity gauge couplings, which vanish asymptotically, take good advantage of this asymptotic splitting procedure. Other studies we are conducting, using a presumably more accurate [24] (converged) two-electronic-state model in the length gauge (this is still a fundamental question being studied for ATD) cannot enjoy the computational benefit of this splitting since $\partial\underline{V}/\partial R$ never vanishes if the field is present.

In the absence of the laser field the bound eigenstates of H_2^+ are well represented as simple products $\Psi_i^0(t,\mathbf{x},R)=e^{-iE_i^0t/\hbar}\mathcal{P}_v\psi_g$ of the bound vibrational wave functions $\mathcal{P}_v(R)$ of H_2^+ in the ground $^2\Sigma_g^+$ electronic-rotational state together with the electronic-rotational channel state $\psi_g(\mathbf{x},R)$, which we emphasize is an implicit function of R. In the presence of the laser field, which is imposed at $t=0$, this stationary state suddenly becomes nonstationary, and can be viewed as undergoing a kind of laser-induced "predissociation" [8,9]. To describe such an experiment we *impose* the initial condition $\Psi(t=0,\mathbf{x},R)=\Psi_i^0(t=0,\mathbf{x},R)=\mathcal{P}_v(R)\psi_g(\mathbf{x},R)$ on the wave function $\Psi(t,\mathbf{x},R)$ in Eq. (10) at $t=0$. The computational quantities of interest are the decay of the initial-state population,

$$P_i(t)=|\langle\Psi(t)|\Psi(t=0)\rangle|^2=\left|\int dR\ G_g(t,R)^*\mathcal{P}_v(R)\right|^2\ , \quad (16)$$

and the relative kinetic-energy distribution of the fragments,

$$P(\varepsilon_k,t)d\varepsilon=(m_H/2p_k)[|G_{g,A}(t,p_k)|^2+|G_{u,A}(t,p_k)|^2]d\varepsilon\ , \quad (17)$$

$k=1,2,\ldots,M$, where $\varepsilon_k=p_k^2/m_H$ is the relative kinetic energy and $G_{g,A}(t,p_k)$ and $G_{u,A}(t,p_k)$ are related to the asymptotic (denoted by subscript A) wave functions in the momentum representation. Note that in the depletion limit $[P_i(t)=0]$ we have $G_{g,A}(t,p_k)\equiv G_g(t,p_k)$ and $G_{g,A}(t,p_k)\equiv G_g(t,p_k)$.

We show later in this section that the decay of the initial-state population and the fragment kinetic-energy distribution are related by a Fourier transform. If $P_i(t)$ decays exponentially then, in the depletion limit as $t\to\infty$ and $P_i(t)\to 0$, the distribution $P(\varepsilon,t)$ as a function of ε consists of a series of Lorentzian peaks, each with identical half-widths $\Gamma/2$ which cumulatively integrate to a unit probability for dissociation. At times less than the depletion limit when $\exp(-\Gamma t/2\hbar)$ has yet to approach zero, $P(\varepsilon,t)$ is of the form [15,25,26]

$$P(\varepsilon,t)=\sum_n\sum_\gamma \frac{P_{n\gamma}(\Gamma/2\pi)\{[1-\exp(-\Gamma t/2\hbar)]^2+4\exp(-\Gamma t/2\hbar)\sin^2[(\varepsilon-\varepsilon_{n\gamma})t/2\hbar]\}}{(\varepsilon-\varepsilon_{n\gamma})^2+\Gamma^2/4} \tag{18}$$

where $P_{n\gamma}$ is the probability of the molecule dissociating into a particular channel defined by the photon number n and electronic-rotational state γ, and $\Gamma/\hbar$ is the decay rate of the initial bound state. The predicted position of the $n\gamma$ peak in the kinetic-energy distribution is $\varepsilon_{n\gamma}=n\hbar\omega+E_i^0+E_{\rm SS}-V_\gamma(R=\infty)$ and represents an n-photon absorption by the initial E_i^0 bound state with resultant dissociation into molecular state γ with asymptotic energy $V_\gamma(R=\infty)$. For H_2^+ both the V_g and V_u potentials vanish identically as $R\to\infty$. An important element in the analysis, in addition to the decay rate and branching ratios, is the ac Stark shift $E_{\rm SS}$ of the initial state which is induced by the applied field. In Sec. IV we explore the possibility of obtaining $P_{n\gamma}$, Γ, and $E_{\rm SS}$ at short times by fitting Eq. (18) to the nondepletion-limit kinetic-energy distribution using a global minimization procedure. The goal is to extend the applicability of the time-dependent method to lower intensities.

B. Time-independent and associated wave-packet method

In this section we will summarize the time-independent method presented in the preceding paper by Mies and Giusti-Suzor [7]. Basically, the decay of the initial-state population in Eq. (16) and the fragment kinetic-energy distribution in Eq. (17) are calculated by constructing a fully quantum-mechanical *molecule-field wave packet*

$$\Omega_i(t)\approx|\bar\alpha(t)\rangle\Psi(t) = \sum_N\sum_n\sum_\gamma\int dE\, e^{-i(N+E)t/\hbar}\Theta_{n\gamma}(N,E,\mathbf{x},R) \times\bar c(N)C_{n\gamma}(E,N)\ , \tag{19}$$

which closely approximates a product of the time-dependent classical field (interaction picture) wave function in Eq. (10) times a coherent radiation state $|\bar\alpha(t)\rangle$,

$$|\bar\alpha(t)\rangle=\sum_N e^{-iNt/\hbar}\bar c(N)|N\rangle \tag{20}$$

with

$$\bar c(N)\equiv\exp(-|\bar\alpha|^2/2)\bar\alpha^N/(N!)^{1/2}\ . \tag{21}$$

This radiation state is the quantum analog of the classical field used in the time-dependent method, with the same expectation value of the maximum electric field operators, $E^0=(8\pi\hbar\omega/V)^{1/2}|\bar\alpha|=(8\pi\hbar\omega\bar N/V)^{1/2}$, where $\bar N=|\bar\alpha|^2$ is the mean number of photons in volume V. This in turn is related to the mean incident intensity of the laser $\bar I=c\hbar\omega\bar N/V$.

The expansion requires a complete set of energy eigenstates $\Theta_{n\gamma}(N,E,\mathbf{x},R)$ of the total molecule-field Hamiltonian

$$H_T=\hbar\omega a^\dagger a+T_R+T_{\hat{\mathbf{R}}}+H_{\rm el}(\mathbf{r},R)+V_{\rm rad}(\mathbf{r},R,\mathbf{A})\ , \tag{22}$$

where $\hbar\omega a^\dagger a$ is the radiation-field Hamiltonian (with eigenstates $|N\rangle$), T_R and $T_{\hat{\mathbf{R}}}$ are the radial and rotational kinetic-energy operators associated with the internuclear coordinate $\mathbf{R}$, $H_{\rm el}(\mathbf{r},R)$ is the electronic Hamiltonian, and the time-independent molecule-field interaction in the radiation-field (velocity) gauge is

$$V_{\rm rad}(\mathbf{r},R,\mathbf{A})=-(e/m_e)\mathbf{p}\cdot\mathbf{A}(\mathbf{r}) +(e^2/2m_e)\mathbf{A}(\mathbf{r})\cdot\mathbf{A}(\mathbf{r})\ , \tag{23}$$

where

$$\mathbf{A}(\mathbf{r})=\left[\frac{2\pi\hbar c^2}{\omega V}\right]^{1/2}(a^\dagger\hat{\mathbf{e}}e^{i\mathbf{k}_\omega\cdot\mathbf{r}}+a\hat{\mathbf{e}}^*e^{-i\mathbf{k}_\omega\cdot\mathbf{r}})$$

is the usual vector potential. In this study we invoke the dipole approximation ($\mathbf{r}=0$) and neglect the $\mathbf{A}\cdot\mathbf{A}$ term in Eq. (23), which couples photon state $|N\rangle$ with states $|N\pm2\rangle$.

We expand the eigenstates $\Theta_{n\gamma}(N,E,\mathbf{x},R)$ of the total Hamiltonian H_T in a product basis of photon number states $|N-n\rangle$, channel states $\psi_\gamma(\mathbf{x},R)$, and nuclear scattering wave functions $F_{n'\gamma',n\gamma}(N,E,R)$, i.e.,

$$\Theta_{n\gamma}(N,E,\mathbf{x},R)=\sum_{n'}\sum_{\gamma'}|N-n'\rangle\psi_{\gamma'}(\mathbf{x},R) \times F_{n'\gamma',n\gamma}(N,E,R)/R\ . \tag{24}$$

These denote a *degenerate* set of multichannel scattering eigenstates of H_T for a given total energy $E_T=E+N\hbar\omega$, and the radial solution vectors $\underline{F}(N,E,R)$, which are calculated using a multichannel close-coupling algorithm with usual scattering boundary conditions, are solutions of the coupled radial equations, $[\underline{T}_R+\underline{U}(R)-\underline{E}]\underline{F}(N,E,R)=0$, where

$$U_{n'\gamma',n\gamma}(R)=\langle N-n'|\langle\psi_{\gamma'}|V_{\rm rad}|\psi_\gamma\rangle|N-n\rangle + \delta_{n,n'}\delta_{\gamma,\gamma'}[V_\gamma(R)-n\hbar\omega] . \quad (25)$$

Rigorously, the summation in Eq. (24) must run over all electronic-rotational channel states $\gamma=\Lambda,J,M$. However, in our model, as in Eq. (10), we include only the two channel states $\psi_g=\phi_g Y_{J,M}$ and $\psi_u=\phi_u Y_{J',M'}$. As discussed earlier, this severe truncation causes great sensitivity to the choice of gauge, and brings into question the accuracy of the results presented in this paper. However, since our purpose here is to demonstrate the excellent agreement one obtains between the time-dependent and time-independent methods of calculation, we ask the reader to accept the limitations imposed by the two-electronic-state approximation.

The index n associated with the radiation number state $|N-n\rangle$ denotes the number of photons that are removed by absorption ($n>0$) or added by stimulated emission ($n<0$) from the initial number state N. E denotes the total energy of the molecule-field system scaled to a given initial number state N, and the asymptotic kinetic energy in dissociation channel $n\gamma$ is

$$\varepsilon_{n\gamma}=E+n\hbar\omega-V_\gamma(R=\infty) . \quad (26)$$

In order to compare with these results to the time-dependent method, we construct an initial wave packet of the form

$$\Omega_i^0(t)=|\bar{\alpha}(t)\rangle\Psi_i^0(t)=|\bar{\alpha}(t)\rangle e^{-iE_i^0t/\hbar}\mathcal{P}_v\psi_g \quad (27)$$

which differs from the ψ_i^0 used in the classical field time-dependent method by the initial presence of the coherent state of the radiation field $|\bar{\alpha}(0)\rangle=\sum_N\bar{c}(N)|N\rangle$. The time evolution of this initial state is given by Eq. (19) with $C_{n\gamma}$ coefficients obtained from the projection,

$$C_{n\gamma}(N,E)=\langle F^*_{0g,n\gamma}(N,E)|\mathcal{P}_v\rangle = \int dR\, F_{0g,n\gamma}(N,E,R)\mathcal{P}_v(R) . \quad (28)$$

Details of this procedure can be found in the preceding paper. In particular we find that in the limit of infinite depletion, as $t\to\infty$, the probability $P_{n\gamma}(E)$ of finding the system dissociated into channel state $|n\gamma\rangle$ after having removed a total of n photons from the coherent radiation field $|\bar{\alpha}\rangle$ is simply related to the projection (28) using $N\approx\bar{N}$,

$$\lim_{t\to\infty}P_{n\gamma}(E)=\sum_N|\bar{c}(N)|^2|C_{n\gamma}(N,E)|^2\approx|C_{n\gamma}(\bar{N},E)|^2 . \quad (29)$$

Since both $V_g(R)$ and $V_u(R)$ vanish as $R\to\infty$, the asymptotic kinetic energy of the fragments in Eq. (26) is simply given as $\varepsilon=E+n\hbar\omega$. The fragment relative kinetic-energy distribution comparable to Eq. (17) as $t\to\infty$ is given by the following sum over molecule-field channel states:

$$P(\varepsilon,t=\infty)=\sum_n\sum_\gamma P_{n\gamma}(E=\varepsilon-n\hbar\omega) . \quad (30)$$

In practice, a close-coupling calculation is performed for many values of E in order to obtain the kinetic-energy distribution. Due to the time-energy uncertainty principle, very rapid dissociation results in a very broad kinetic-energy distribution, and calculations must be performed for many n and over a large range of energies. One can determine whether $P(\varepsilon)$ has been calculated at all important n, γ, and E by determining whether the kinetic-energy distribution integrates to one. On the other hand, if dissociation is slow the kinetic-energy distribution consists of narrow peaks which are Lorentzian in form, and the positions, widths, and heights of the peaks can be determined by calculating $P_{n\gamma}(E)$ at only a few energies.

By using the expressions (27) and (19) for $\Omega_i^0(t)$ and $\Omega_i(t)$ one can evaluate the decay of the initial-state population, $P_i(t)=|\langle\Omega_i^0(t)|\Omega_i(t)\rangle|^2$. If we average over one optical cycle we find that this reduces to a relatively simple expression

$$P_i(t)=\left|\sum_n\sum_\gamma\int dE\,P_{n\gamma}(E)\exp\left[\frac{i(E_i^0-E)t}{\hbar}\right]\right|^2 , \quad (31)$$

which is the square modulus of the Fourier transform of the fragment kinetic-energy distribution given in Eq. (29). Note that if $P_{n\gamma}(E)$ is Lorentzian,

$$P_{n\gamma}(E)=(P_{n\gamma}\Gamma/2\pi)/[(E-\epsilon_{n\gamma})^2+(\Gamma/2)^2] , \quad (32)$$

then $P_i(t)$ decays exponentially:

$$P_i(t)=\exp(-\Gamma t/\hbar) . \quad (33)$$

The short-time line-shape function, Eq. (18), is obtained by substituting Eq. (33) into Eq. (31) and applying the inverse Fourier transform with the limits of integration from $t=0$ to $t=t_f$.

IV. RESULTS AND DISCUSSION

In this section we calculate the fragment kinetic-energy distribution and the decay of the initial bound-state population, using both the time-dependent and time-independent methods, under conditions that result in either very rapid, moderately rapid, or slow dissociation. By rapid dissociation we mean that the dissociation rate is large enough that the depletion limit [$P_i(t_f)\approx0$] can be reached by the time-dependent method in a computationally acceptable length of time ($t_f<5000$ optical cycles). Very rapid dissociation implies that the kinetic-energy distribution is broad, non-Lorentzian, and with adjacent kinetic-energy peaks possibly overlapping. By moderately rapid we imply that the decay is essentially exponential as in the slow dissociation case, with well-resolved kinetic-energy peaks associated with specific Floquet channels n. In the slow dissociation limit it is numerically inconvenient to carry the calculations through to complete dissociation. However, this computational restriction can be circumvented if the decay is purely exponential by fitting Eq. (18) to the fragment kinetic-energy distribution.

A. Slow and moderately rapid dissociation

For our study of slow and moderately rapid dissociation we use the ground vibrational state ($v=0$) as the initial state, and a laser field of wavelength $\lambda=3297$ Å, for which the three-photon transition is near resonance, and intensities of either $I=7.0\times10^{12}$, 1.4×10^{13}, or 5.6×10^{13} W/cm^2. The $G_g(t,R)$ and $G_u(t,R)$ components of the time-dependent wave function [see Eq. (10)] are propagated on an $N=256$ point grid of length $L=25a_0$, the time step is $\Delta t=\pi/20\omega$, and $G_g(t,R)$ and $G_u(t,R)$ are split into interaction and asymptotic region pieces (see Ref. [15]) whenever their modulus exceeds $10^{-5}a_0^{-1/2}$ near the end of the grid. The asymptotic region pieces of the wave function are propagated on an $N=8192$ or 16 384 point momentum grid in order to obtain a high-resolution kinetic-energy distribution. For the time-independent calculation the wave function [Eq. (24)] is expanded in 25 photon states around $|\bar{N}\rangle$.

The bare (solid curves) and dressed (dashed curves) molecule-plus-field potential-energy curves for $I=5.6\times10^{13}$ W/cm^2 and $\lambda=3297$ Å, for photon states in the vicinity of $|\bar{N}\rangle$, are shown in Fig. 1. The bare molecule-plus-field curves are the R-dependent eigenvalues of $T_{\hat{\mathbf{R}}}+H_{\rm el}+\hbar\omega a^\dagger a$, with eigenstates $|\bar{N}-n\rangle\psi_\gamma(\mathbf{x},R)$, and the dressed molecule-plus-field curves are eigenvalues of $H_T-T_R=T_{\hat{\mathbf{R}}}+H_{\rm el}+\hbar\omega a^\dagger a+V_{\rm rad}(\mathbf{r},R,\mathbf{A})$, whose eigenstates are linear combinations of $|\bar{N}-n\rangle\psi_\gamma(\mathbf{x},R)$, found by diagonalizing H_T-T_R in that basis.

Several features of the molecule-plus-field potential energy curves are worth identifying. Avoided crossings occur at internuclear separations R satisfying $V_u(R)+n'\hbar\omega=V_g(R)+n\hbar\omega$, whenever $n-n'$ is an odd number. Starting from a bound vibrational state in the $|\bar{N}\rangle\psi_g$ diabatic channel, the system undergoes a kind of laser-induced predissociation [7–10], and the fragments may undergo a series of such curve crossings as they proceed to large separation. The larger $n-n'$ is the higher the order of the molecule-field interaction and the less severe the avoided crossing. The avoided crossing at $R=3.6a_0$ satisfies $n-n'=1$ and has the effect of pulling down the barrier to dissociation. This "laser-induced bond softening" [5] affects the upper vibrational states more than the lower vibrational states because the bottom of the potential well remains relatively undistorted, although it is ac Stark shifted downward in energy. Since the shift of the bound state is downward relative to the asymptotic potential energy, the fragments have less kinetic energy than would be expected from energy conservation, which predicts $\varepsilon_{n\gamma}=n\hbar\omega+E_i^0-V_\gamma(R=\infty)$.

The exponential decay of the initial $v=0$ bound-state population, shown in Fig. 2 for $I=5.6\times10^{13}$ W/cm^2, is due to the $n-n'=3$ avoided crossing occurring at the H_2^+ equilibrium separation $R=2a_0$. Since this is third order in the laser-molecule coupling the avoided crossing does not distort greatly the dressed-state potential curves and, at least for $I=7\times10^{12}$ and 1.4×10^{13} W/cm^2, the field-free $v=0$ vibrational wave function is almost exclusively projected onto the $v=0$ dressed-state eigenfunction and not other bound or continuum dressed states. The rapid oscillation in $P_i(t)$ seen in Fig. 2 is due to the mixing of states during the optical cycle—the minimum occurring when $\cos(\omega t)$ equals $+1$ or -1. Shown for comparison in Fig. 2 is the exponential decay $P_i(t)=\exp(-\Gamma t/\hbar)$ with Γ determined by fitting Eq. (18)

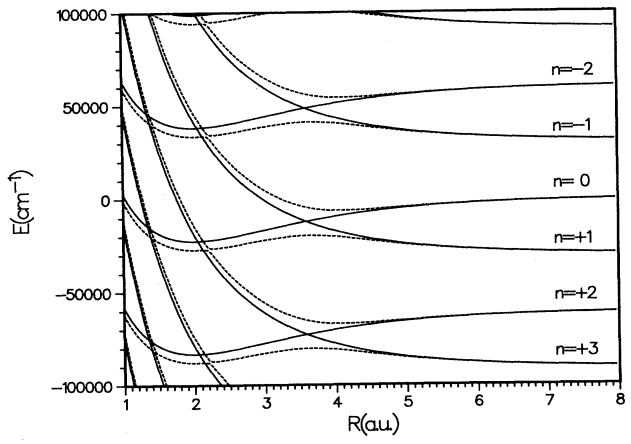

FIG. 1. Bare (solid curves) and dressed (dashed curves) molecule-plus-field potential energy curves, for $\lambda=3297$ Å and $I=5.6\times10^{13}$ W/cm^2. Shown are curves which asymptotically correlate with photon number states $|\bar{N}-n\rangle$ in the vicinity of $|n|\le3$. Excellent convergence of time-independent close-coupled calculations was obtained by including a set of 25 number states with $|n|\le12$. $E_{n=0,v=0}$(bare)$=-21\,298$ cm^{-1}. $E_{n=0,v=0}$(dressed)$\approx-25\,998$ cm^{-1}.

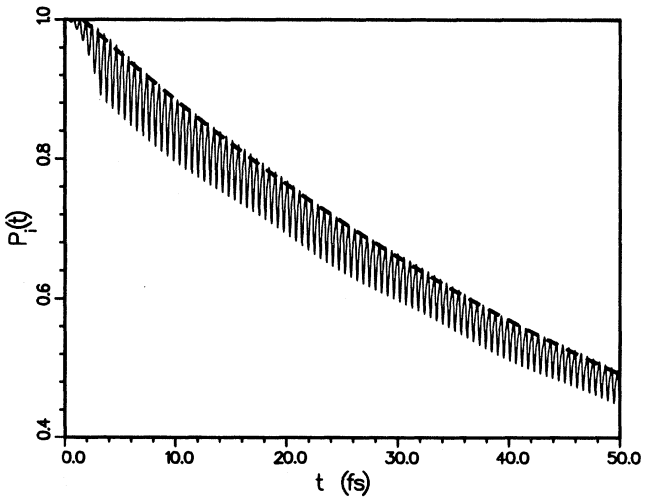

FIG. 2. Decay of the initial-state population, for $\lambda=3297$ Å, $I=5.6\times10^{13}$ W/cm^2, and $v=0$, calculated using the time-dependent method (solid curve) along with the exponential decay $P_i(t)=\exp(-\Gamma t/\hbar)$ (dashed curve), where $\Gamma=78.0$ cm^{-1} was determined by fitting Eq. (18) to the fragment kinetic-energy distribution. The broken curve has been shifted by 1.5τ to compensate for the 3τ turn-on time of the time-dependent calculation.

to the fragment kinetic-energy distribution (dashed curve).

Two peaks corresponding to $n=2$, $\gamma=g$ and $n=3$, $\gamma=u$ are seen in the short-time fragment kinetic-energy distributions shown in Fig. 3, for $t_f=500\tau$ ($\tau=2\pi/\omega$), and using an intensity of (a) $I=7.0\times10^{12}$ W/cm^2, (b) $I=1.4\times10^{13}$ W/cm^2, and (c) $I=5.6\times10^{13}$ W/cm^2. In Fig. 3 the points represent the kinetic-energy distribution

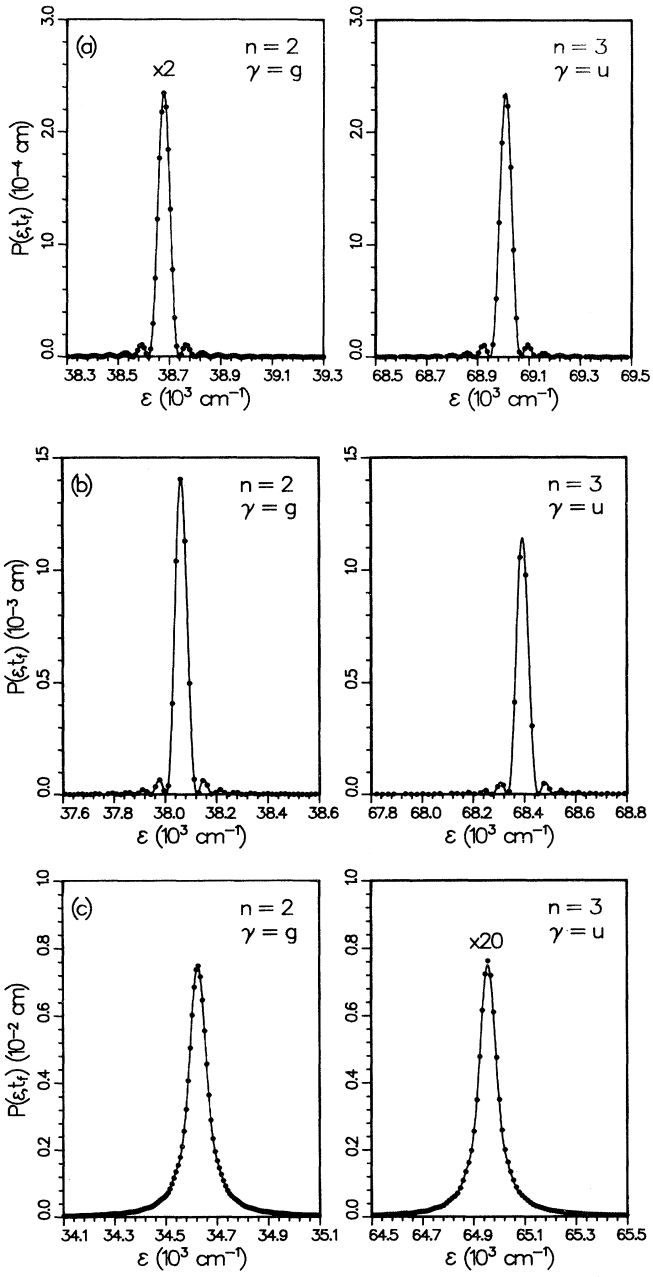

FIG. 3. Short-time ($t=500\tau$) fragment kinetic-energy distributions calculated using the time-dependent method (points), and the fit of the short-time line-shape function, Eq. (18), to these points (solid curves), for $\lambda=3297$ Å, $v=0$, and intensities of (a) $I=7.0\times10^{12}$ W/cm^2; (b) $I=1.4\times10^{13}$ W/cm^2; and (c) $I=5.6\times10^{13}$ W/cm^2.

calculated by the time-dependent method [Eq. (17)] and the curves are fits of Eq. (18). The $n=3$ peak is produced by three-photon absorption to the unbound $^2\Sigma_u^+$ state. As the molecule falls apart, stimulated emission occurs at a separation $R=3.6a_0$ where the difference between the $V_u(R)$ and $V_g(R)$ potentials equals the photon energy. In Fig. 1 this appears as an avoided crossing at $R=3.6a_0$ in the dressed-state potential curves labeled asymptotically as $n=3$ and 2. The decrease in the $G_u(t,R)$ amplitude and the increase in the $G_g(t,R)$ amplitude between $3a_0$ and $4a_0$—seen in Fig. 4 for the $I=5.6\times10^{13}$ W/cm^2 example—is further evidence for this interpretation of the origin of the $n=2$ peak. At lower intensity the stimulated emission is less efficient and more flux remains in the $n=3$, $\gamma=u$ channel. Note that the short-time fragment kinetic-energy distribution shown in Figs. 3(a) and 3(b) displays oscillations predicted by the line-shape function Eq. (18) for times less than the depletion limit.

We now explore the possibility of fitting Eq. (18) to the short-time fragment kinetic-energy distribution in order to accurately determine the decay rate $\Gamma/\hbar$, the branching ratio $P_{n=2,g}/P_{n=3,u}$, and the ac Stark shift E_{SS} at times much less than the depletion limit. We use the same initial state and wavelength used above, and intensities of $I=7\times10^{12}$ and 1.4×10^{13} W/cm^2, which result in slow dissociation, in addition to $I=5.6\times10^{13}$ W/cm^2, which results in what we term moderately rapid dissociation. Values of the decay rate, branching ratio, ac Stark shift, and the final initial-state population, for the three intensities and propagation times ranging from 25τ to 1000τ, are tabulated in Table I. Except where noted, the time-dependent interaction was ramped on (and off) over three optical cycles. Values of the quantities obtained using the time-independent method are listed for comparison. Upon inspection of Table I one sees that, except for the high-intensity decay rate, the long-time time-dependent and time-independent results are in good

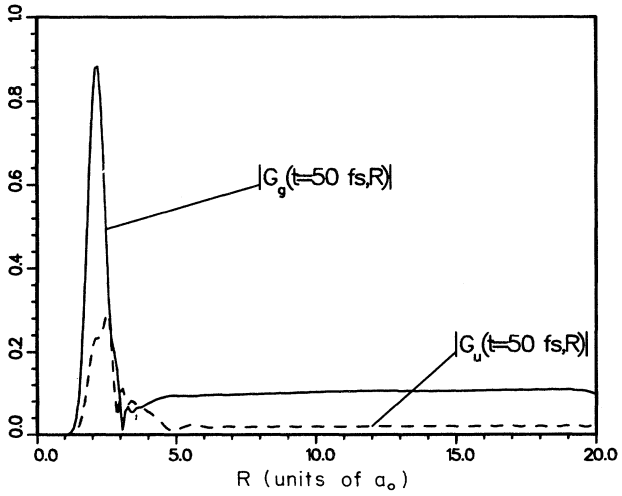

FIG. 4. The nuclear wave functions $G_g(t,R)$ (solid curve) and $G_u(t,R)$ (dashed curve) associated with the ψ_g and ψ_u channel states at $t=50$ fs for $\lambda=3297$ Å, $I=5.6\times10^{13}$ W/cm^2, and $v=0$.

agreement. The short-time and long-time time-dependent results are in better agreement as the intensity is decreased, which is the desired trend if one wishes to extend the time-dependent method to lower intensities.

Table I displays several trends in the values of the calculated quantities as a function of intensity and propagation time. For example, the branching ratio increases with propagation time, with the greatest change occurring at high intensity. This is due to the average intensity being lower for short propagation times, where by average intensity we mean the intensity averaged over the turn-on, constant, and turn-off periods of $f(t)$. The amount of stimulated emission and therefore the branching ratio decreases with decreasing average intensity. The difference between the average intensity and the maximum intensity increases with maximum intensity, thus the increased sensitivity of the $I=5.6\times10^{13}$ W/cm^2 branching ratio to the propagation time (15% error for $t_f=50\tau$), compared to the $I=1.4\times10^{13}$ W/cm^2 (6.5% error) and $I=7.0\times10^{12}$ W/cm^2 (3% error) cases. A slight improvement is obtained in the $I=5.6\times10^{13}$ W/cm^2 calculation by decreasing the turn-on and turn-off periods from three to one optical cycles (29% versus 34% error for $t_f=25\tau$), although one runs the risk of introducing transients into the kinetic-energy distributions if the turn-on and turn-off times are made too short.

Trends in the decay rate of the initial bound state as a function of the propagation time are different for the three intensities, i.e., the decay rate increases for $I=7.0\times10^{12}$ W/cm^2, remains constant for $I=1.4\times10^{13}$ W/cm^2, and decreases for $I=5.6\times10^{13}$ W/cm^2 as t_f increases. The latter case is contrary to the argument that the average intensity increases with propagation time, and that the decay rate increases with average intensity, therefore one expects the decay rate to increase with propagation time. Another possible source of error at short times may be due to a fast decay component, which would appear first in the kinetic-energy distribution. In the language of time-independent theory the fast decay component results from a nonzero projection of the initial field-free bound-state ave function onto high-lying bound or continuum dressed states. While possibly small in magnitude, the fast decay component may at short times make a large relative contribution to the fragment kinetic-energy distribution compared to the slow decay component. The fact that the fast decay component increases in magnitude relative to the slow decay component, as the intensity increases, may explain both the unexpected trend in the $I=5.6\times10^{13}$ W/cm^2 calculation and why the values of the decay rate calculated by the time-dependent and time-independent methods differ by several percent at this intensity. Of course, the line-shape expression Eq. (18) assumes that there is only one decay rate. Note that the decay rate scales as I^3 for the lowest and intermediate intensities, as expected from perturbation theory if dissociation is due to a three-photon pro-

TABLE I. Parameters of the short-time line-shape function fit to the fragment kinetic-energy distribution as a function of intensity and propagation time.

Method[a]	I (10^{12} W/cm^2)	t_f (τ)	$P_i(t_f)$	$P_{n=2,g}/P_{n=3,u}$	Γ (cm^{-1})	E_{SS} (cm^{-1})
TD	7.0	50	0.998	0.483	0.205	−626
TD	7.0	100	0.990	0.493	0.207	−627
TD	7.0	200	0.980	0.498	0.207	−628
TD	7.0	300	0.969	0.500	0.207	−628
TD	7.0	500	0.950	0.500	0.207	−628
TD	7.0	1000	0.902	0.498	0.208	−628
TI	7.0	∞	0.0	0.501	0.211	−633
TD	14.0	50	0.983	1.16	1.62	−1247
TD	14.0	100	0.967	1.20	1.62	−1245
TD	14.0	200	0.935	1.22	1.62	−1245
TD	14.0	300	0.904	1.23	1.62	−1245
TD	14.0	500	0.846	1.24	1.62	−1245
TD	14.0	1000	0.715	1.25	1.62	−1245
TI	14.0	∞	0.0	1.26	1.64	−1251
TD	56.0	25	0.660	13.3	80.2	−4737
TD[b]	56.0	25	0.661	14.4	79.9	−4695
TD	56.0	50	0.441	17.2	79.1	−4692
TD	56.0	100	0.195	19.0	79.0	−4684
TD	56.0	200	0.040	19.8	78.0	−4682
TD	56.0	300	0.008	19.8	77.9	−4682
TD	56.0	500	0.0003	20.3	77.9	−4682
TD	56.0	1000	0.0	20.3	78.0	−4682
TI	56.0	∞	0.0	20.2	79.4	−4700

[a]Calculated using the time-dependent (TD) or time-independent (TI) method.
[b]For this calculation the interaction was ramped on (and off) in 1τ ($\tau=2\pi/\omega$), for all others 3τ.

cess. This is not the case for $I=5.6\times10^{13}$ W/cm^2, which produces a decay that is slower than predicted, perhaps because the initial state has been Stark shifted off resonance.

The ac Stark shift, tabulated in the last column of Table I, is first order in intensity and appears to be relatively insensitive to propagation time. The agreement between the time-dependent and time-independent results for the ac Stark shift is especially good if one considers how small the difference is compared to the photon energy (30 033 cm^{-1}). Although this self-consistency between the two methods is the main message of this paper, it must be remembered (see Sec. II) that both calculations are probably converging on a result that is only partially valid for the H_2^+ system. These calculations are restricted to only two electronic-rotational states of H_2^+ and the magnitude of these shifts which agree so well between the two sets of calculations is very sensitive to the choice of gauge.

B. Very rapid dissociation

In our final example we examine further the idea of fast and slow decay components in intense-field photodissociation. We use the $v=2$ vibrational state as the initial state, which is subjected to a laser of intensity $I=2\times10^{14}$ W/cm^2 and wavelength $\lambda=2480$ Å. This example falls in the category of very rapid dissociation, i.e., the widths of the peaks in the fragment kinetic-energy distribution are broader than the vibrational spacing. The grid length and spacing for the time-dependent calculation is the same as in Sec. IV A, and we use 40 time steps per optical cycle. In the time-independent calculation the wave function is expanded in 25 photon number states around $|\bar{N}\rangle$.

The reason why dissociation is very rapid becomes apparent upon inspection of the bare (diabatic) and dressed (adiabatic) potential-energy curves, shown in Fig. 5, for this choice of intensity and wavelength: the shorter wavelength causes the curve crossing of the $n=0$ and 1 bare potentials to be somewhat closer to the equilibrium position, and the strong molecule-field interaction greatly distorts the dressed-state curves. Also shown in Fig. 5 are the positions of the few vibrational levels supported by the adiabatic potentials. These states can dissociate via either the avoided crossing near $R=2$ a.u., which leads asymptotically to $n=2$, $\gamma=g$, or by tunneling through the barrier, which leads asymptotically to $n=1$, $\gamma=u$. The bare $n=0$, $v=2$ initial state, which lies closer to the top of the adiabatic potential well than the $v=0$ state in the example in Sec. IV A, is projected onto continuum states as well as these bound dressed states.

Evidence of the projection onto the adiabatic $v_A=1,2$, and rather broad $v_A=3$ vibrational levels is seen in Fig. 6, where the total line shape calculated using the time-independent method is plotted for energies in the vicinity of these levels. This contribution to the kinetic-energy distribution accounts for only about 80% of the initial population, and gives rise to the nonexponential decay curve presented in the preceding paper [7], which is not normalized to unity at $t=0$. The missing population can

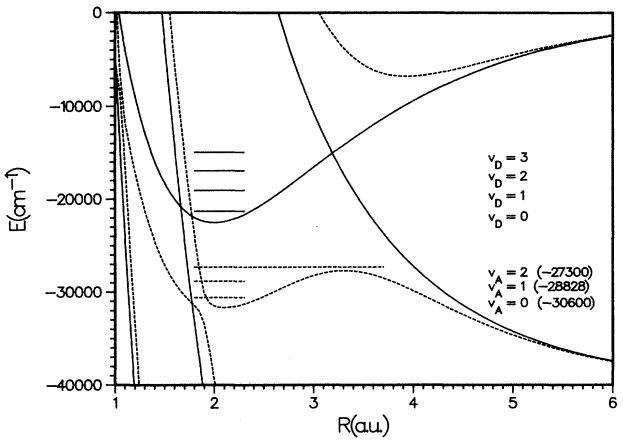

FIG. 5. Bare (solid curves) and dressed (dashed curves) molecule-plus-field potential-energy curves for photon number states $|\bar{N}-n\rangle$ in the vicinity of $n=0$, for $\lambda=2480$ Å, and $I=2\times10^{14}$ W/cm^2. The initial bare $n=0$, $v=2$ state at $E=-16\,949$ cm^{-1} is primarily projected onto adiabatic dressed $n=0$ vibrational states with $E_1\approx-28\,825$ cm^{-1}, $E_2\approx-27\,300$ cm^{-1}, and a broad $E_3\approx-26\,000$ cm^{-1}.

be associated with very fast decaying components obtained from the projection of the initial wave function onto the continuum and the high-lying dressed vibrational states distributed over a broad range of total energies. These missing components have been carefully calculated, and are presented in Fig. 7. The time-independent calculations can now account for over 99% of the population.

The existence of multiple decay components can be seen in Fig. 8 where we plot $P_i(t)$ calculated by the time-dependent (solid curve) and time-independent (dashed curve) methods. $P_i(t)$ displays a very rapid drop due to a

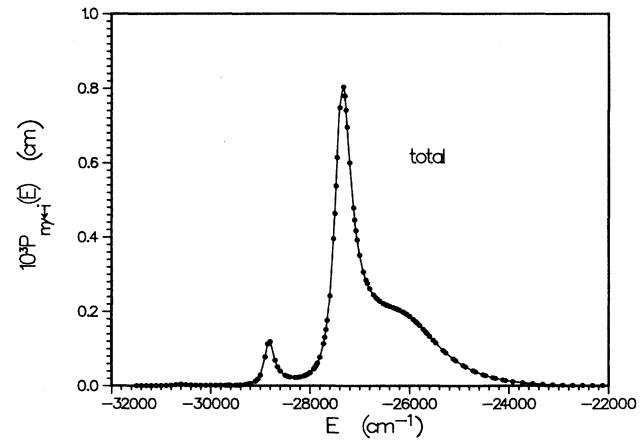

FIG. 6. Total line shape for $v=2$ initial state for $\lambda=2480$ Å, and $I=2\times10^{14}$ W/cm^2, in vicinity of adiabatically dressed $v_A=1$, 2, and 3 vibrational levels defined by $n\approx0$ in Fig. 5. The integrated probability in this region is approximately 80%. The remaining distribution is shown in Fig. 7.

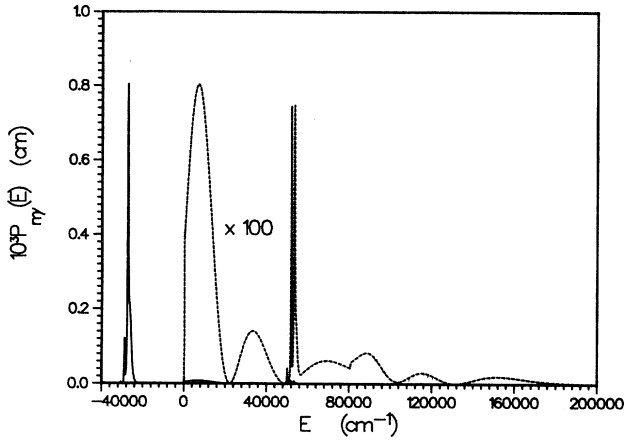

FIG. 7. Total line shape for $v=2$ initial state for $\lambda=2480$ Å, and $I=2\times10^{14}$ W/cm^2. Approximately 20% of the initial distribution is distributed throughout a broad total energy range from $E=0$ to 200 000 cm^{-1}.

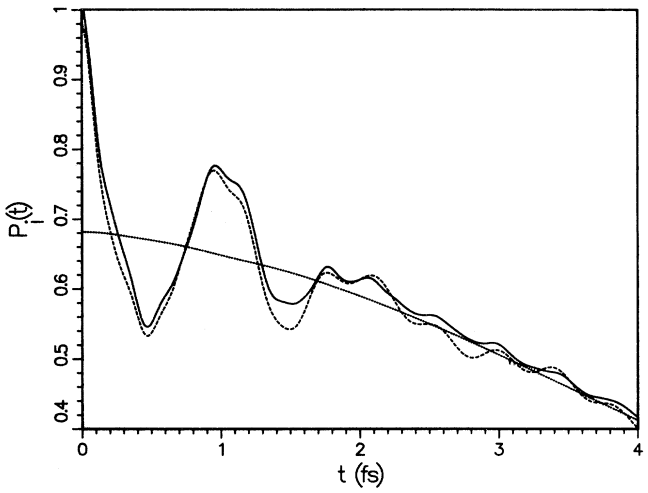

FIG. 9. Short-time behavior of the decay of the initial-state population shown in Fig. 8. The dotted curve excludes the components with $E>0$ in Fig. 7.

high total energy continuum component, which decays within the first several optical cycles. The broad $v_A=3$ component decays within roughly the first ten optical cycles, and the narrower $v_a=0$, 1, and 2 components are depleted within roughly 50 optical cycles. The oscillations in $P_i(t)$ are a consequence of the overlap of the peaks in the kinetic-energy distribution: interference results from the ability of two different vibrational states to produce fragments with the same kinetic energy.

$P_i(t)$ at short times is shown in more detail in Fig. 9. Without including the components with $E\geq0$ in Fig. 7 the wave-packet expression Eq. (31) gives the smooth dotted decay curve in Fig. 9. However, by including the remaining components the wave packet produces a complicated interference pattern shown by the dashed curve. It is a tedious but simple matter to associate these oscillations with various features in Fig. 7. However, what is most pleasing is to find this very excellent agreement with the time-dependent decay curve shown by the solid curve. The solid curves in both Figs. 8 and 9 were obtained by averaging $P_i(t)$ of the time-dependent calculations over the initial phase δ of the time-dependent field $E^0\cos(\omega t+\delta)$. This gave the best agreement with the time-independent result: $\delta=0$ resulted in too much continuum component and $\delta=\pi/2$ too little, as did turning on the interaction over several optical cycles.

In Fig. 10 we plot the depletion-limit fragment kinetic-energy distributions corresponding to these decay curves, calculated using the time-independent method

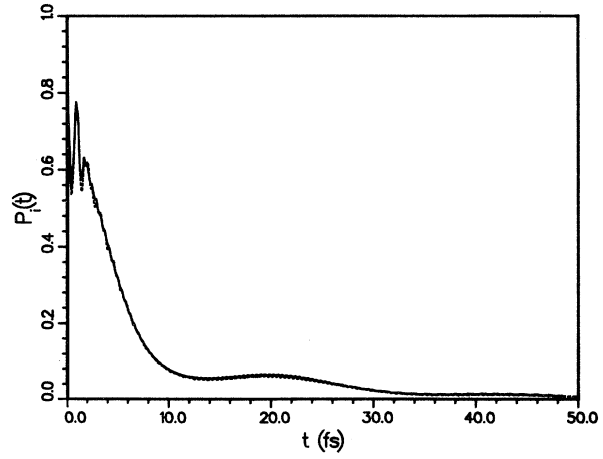

FIG. 8. Decay of the initial-state population calculated using the phase-averaged time-dependent method (solid curve) and the time-independent method (dashed curve), for $\lambda=2480$ Å, $I=2\times10^{14}$ W/cm^2, and $v=2$.

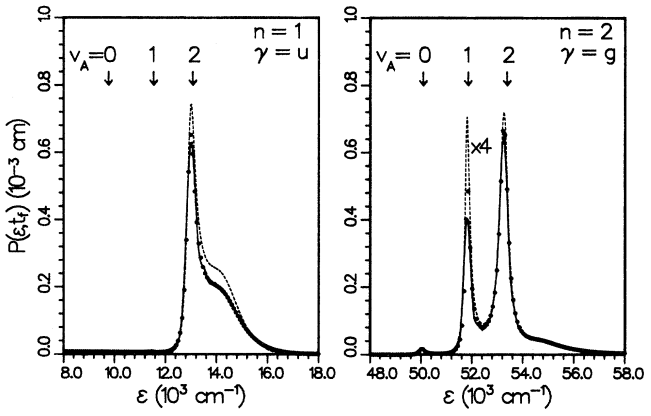

FIG. 10. Fragment relative kinetic-energy distribution calculated using the time-independent method (points), the time-dependent method averaged over the initial phase of the field (solid curve), and the time-dependent method with the field ramped on over three optical cycles (dashed curve), for $\lambda=2480$ Å, $I=2\times10^{14}$ W/cm^2, and $v=2$. The left panel is predominantly $P_{n=1,u}$ contribution, the right panel is predominantly $P_{n=2,g}$ contribution, and the peaks are labeled according to the dressed vibrational state they originated from.

(points), the time-dependent method with the interaction ramped on over three optical cycles (dashed curve), and the time-dependent method using a square pulse shape and averaging over the initial phase of the field (solid curve). Unlike the $\lambda=3297$ Å, $v=0$ example of Sec. IV A, the one- and two-photon peaks have dissimilar, non-Lorentzian line shapes. The time-independent result was obtained by rearranging the various $n\gamma$ components of the distribution shown in Fig. 7 according to their kinetic energy $\varepsilon_{n\gamma}=E+n\hbar\omega-V_\gamma(R=\infty)$. As a result of the high intensity, the time-independent calculations must be performed over a range of total energy of more than 200 000 cm^{-1} (as evidenced in Fig. 7), and much bookkeeping is required to construct the kinetic-energy distribution.

The positions of the peaks corresponding to the decay of the dressed vibrational states are labeled to indicate their relative contribution. The distributions shown in the first and second panels represent dissociation via mainly the $n=1$ and 2 channels, respectively, although at this intensity many different channels contribute, over a broader range of kinetic energy than that shown. Due to the time-energy uncertainty principle, which manifests itself as the Fourier transform in Eq. (31), rapid decay components appear as broad features in the kinetic-energy distribution. In the example shown in Fig. 10, the initial field-free $v=2$ bound state is projected onto the $v_A=0-3$ dressed bound states as well as the continuum. The $v_A=0$ and 1 dressed-state components decay via the two-photon channel, and the $v_A=2$ and 3 components decay via mainly the one-photon channel, but also the two-photon channel. Also visible in the first panel of Fig. 10 is a flat, high total energy continuum contribution, which extends from near zero kinetic energy to more than 10 000 cm^{-1}. This component of the kinetic-energy distribution is associated with the very rapid decay of $P_i(t)$ in the first several optical cycles.

In Fig. 10 one sees that the fragment kinetic-energy distribution calculated using the time-independent method (points) agrees well with the square pulse time-dependent calculation (solid curve) that was averaged over ten values of the initial phase of the field, but not as well with the time-dependent calculation using an interaction that was ramped on over three optical cycles (dashed curve): the phase-averaged time-dependent calculation slightly underestimates the contribution from the $v_A=1$ and 2 levels; whereas the ramped-on time-dependent calculation substantially overestimates the contribution from the $v_A=1$ and 2 levels and the $n=1$, $v_A=3$ level. On the other hand, the ramped-on calculation underestimates the broad low kinetic-energy continuum component, which is slightly overestimated by the phase-averaged calculation. The good agreement between the time-independent and phase-averaged time-dependent result is not surprising considering the fact that the decays of the initial-state population are in good agreement, and that the decay and kinetic-energy distribution are related by a Fourier transform. Finally, we note that ramping on the interaction over several optical cycles works well at lower intensities, because there is no rapid decay component, and that performing the calculation with different values of the initial phase and then averaging is both unnecessary and very inefficient computationally if dissociation is slow.

V. CONCLUSION

In this paper we explored the complementarity of time-dependent and time-independent methods in the study of intense-field photodissociation of H_2^+ by calculating the fragment kinetic-energy distribution and initial-state population decay for several intensities, wavelengths, and initial vibrational states. The time-dependent method propagates the wave function in time by the repeated application of a short-time propagator, and it assumes a classical, time-dependent interaction for which one is free to choose how the field is turned on and off. On the other hand, the time-independent method projects the initial bound-state wave function onto eigenstates of the total molecule-plus-field Hamiltonian, and the process becomes essentially one of laser-induced predissociation. The time dependence is eliminated by either using a classical molecule-field interaction and then integrating over the optical cycle, or by using a quantum interaction and assuming that the field can be described by an average photon number state $|\bar{N}\rangle$. Since the time dependence has been eliminated, one cannot easily account for different pulse shapes, i.e., different ways of turning on and off the field.

The time-independent method is more efficient at low to moderate intensities because few molecule-plus-field basis functions are needed in the wave-function expansion, and the positions, heights, and widths of peaks in the kinetic-energy distribution can be determined by performing the calculation at only a few values of the total energy and then fitting the results to Lorentzian line-shape functions. On the other hand, the time-dependent method, as usually applied, is inefficient at low to moderate intensities because the wave function must be propagated for many time steps before the depletion limit is reached. In this paper we successfully applied a procedure for obtaining depletion-limit quantities at short times by fitting a short-time line-shape function to the nondepletion-limit fragment kinetic-energy distribution using a global minimization procedure. Values of the decay rate, branching ratio, and ac Stark shift, calculated using the fitting procedure, were in very good agreement with those calculated with the time-independent method at the lowest intensities studied. At high intensities the time-independent method becomes less efficient because many molecule-plus-field basis functions must be included in the wave-function expansion and the calculation must be carried out over a wide range of total energy.

At the highest intensities studied we found evidence for multiple decay components in the fragment kinetic-energy distribution and in the decay of the initial-state population. In the language of the time-independent theory, these decay components result from a nonzero projection of the initial bound state onto continuum as well as high- and low-lying dressed vibrational states. The rapidly decaying continuum component is very sensitive to how the time-dependent interaction is turned on,

and can cause differences between the time-dependent and time-independent results. We found that these differences were minimized if one performed a series of time-dependent calculations using a square pulse shape with a series of initial phases, and then performs a subsequent average of the results over this phase. This is very similar in philosophy to the implied average over an optical cycle that is at the heart of the Floquet-like methods. The computationally more efficient procedure of turning on the interaction over several optical cycles and not phase averaging resulted in an increase in the slow decay contribution and a decrease in the fast decay contribution to the fragment kinetic-energy distribution, compared with the time-independent result.

In conclusion, we wish to stress that even under conditions for which it is very difficult to perform the time-independent calculation, e.g., at very high intensity or for pulsed excitation, the dressed molecule-plus-field potential energy curves—which are easily calculated—provide much qualitative insight into such processes as laser-induced bond softening, laser-induced bound states, ac Stark shifts, and the intensity dependence of ATD branching ratios and photodissociation rates.

ACKNOWLEDGMENTS

We acknowledge with gratitude many helpful discussions with Annick Giusti-Suzor. Research was supported in part by a NATO grant for International Collaboration in Research One of us (F.H.M.) acknowledges that this work was sponsored in part by the U.S. Air Force Office of Scientific Research.

[1] P. Agostini, F. Fabre, G. Mainfray, and N. K. Rahman, Phys. Rev. Lett. **42**, 1127 (1979); F. Fabre, G. Petite, P. Agostini, and M. Clement, J. Phys. B **15**, 1353 (1982); P. Kruit, J. Kimmer, H. G. Muller, and M. J. Van der Wiel, Phys. Rev. A **28**, 248 (1983); L. A. Lompre, A. L'Huillier, G. Mainfray, and C. Manus, J. Opt. Soc. Am. B **2**, 1906 (1985).

[2] C. Cornaggia, D. Normand, J. Morellec, G. Mainfray, and C. Manus, Phys. Rev. A **34**, 807 (1986).

[3] K. Codling, L. J. Frasinski, and P. A. Hatherly, J. Phys. B **21**, L433 (1988).

[4] P. H. Bucksbaum, A. Zavriyev, H. G. Muller, and D. W. Schumacher, Phys. Rev. Lett. **64**, 1883 (1990).

[5] A. Zavriyev, P. H. Bucksbaum, H. G. Muller, and D. W. Schumacher, Phys. Rev. A **42**, 5500 (1990).

[6] N. B. Delone and V. P. Krainov, *Atoms in Strong Light Fields* (Springer, Berlin, 1984), p. 45.

[7] F. H. Mies and A. Giusti-Suzor, preceding paper, Phys. Rev. A **44**, 7547 (1991).

[8] A. Giusti-Suzor, X. He, O. Atabek, and F. H. Mies, Phys. Rev. Lett. **64**, 515 (1990).

[9] A. D. Bandrauk and M. L. Sink, J. Chem. Phys. **74**, 1110 (1981); A. D. Bandrauk and O. Atabek, Adv. Chem. Phys. LXII, 823 (1989); A. D. Bandrauk and J.-M. Gauthier, J. Opt. Soc. Am. B **7**, 1420 (1990).

[10] S.-I. Chu, J. Chem. Phys. **75**, 2215 (1981); Adv. At. Mol. Phys. **31**, 197 (1985); Adv. Chem. Phys. LXII, 739 (1989).

[11] K. C. Kulander, Phys. Rev. A **35**, 445 (1987); **36**, 2726 (1987); **38**, 778 (1988).

[12] R. Heather and H. Metiu, J. Chem. Phys. **88**, 5496 (1988).

[13] J. Parker and C. R. Stroud, Jr., Phys. Rev. A **41**, 1602 (1990).

[14] L. A. Bloomfield, J. Opt. Soc. Am. B **7**, 472 (1990); K. C. Kulander and B. W. Shore, *ibid.* **7**, 502 (1990); Q. Su and J. H. Eberly, *ibid.* **7**, 564 (1990); K. J. La Guttuta, *ibid.* **7**, 639 (1990); L. A. Collins and A. L. Merts, *ibid.* **7**, 647 (1990); M. S. Pindzola, G. J. Bottrell, and C. Bottcher, *ibid.* **7**, 659 (1990); R. Blumel, U. Smilansky, *ibid.* **7**, 664 (1990); C. Cerjan, *ibid.* **7**, 680 (1990); J. K. Liakos and M. Horbatsch, *ibid.* **7**, 685 (1990).

[15] R. W. Heather, Comput. Phys. Commun. **63**, 446 (1991).

[16] P. L. DeVries, Comput. Phys. Commun. **63**, 95 (1991); K. J. Schafer, *ibid.* **63**, 427 (1991); S. I. Chu and T. F. Jiang, *ibid.* **63**, 482 (1991); K. C. Kulander and T. N. Rescigno, *ibid.* **63**, 523 (1991); F. J. Lin and J. T. Muckerman, *ibid.* **63**, 538 (1991).

[17] R. Loudon, *The Quantum Theory of Light* (Clarendon, Oxford, 1983), p. 148.

[18] S. W. Allendorf and A. Szöke, Phys. Rev. A **44**, 518 (1991).

[19] D. R. Bates, J. Chem. Phys. **19**, 1122 (1951).

[20] C. Cohen-Tannoudji, J. Dupont-Roc, and G. Grynberg, *Photons and Atoms* (Wiley, New York, 1989), p. 320.

[21] C. Cohen-Tannoudji, J. Dupont-Roc, and G. Grynberg, Ref. [20], p. 324.

[22] J. A. Fleck, Jr., J. R. Morris, and M. D. Feit, Appl. Phys. **10**, 129 (1976); M. D. Feit, J. A. Fleck, Jr., and A. Steiger, J. Comput. Phys. **47**, 412 (1982); M. D. Feit and J. A. Fleck, Jr., J. Chem. Phys. **81**, 3722 (1984).

[23] J. Alvarellos and H. Metiu, J. Chem. Phys. **88**, 4957 (1988).

[24] H. G. Muller (private communication). Conclusion based on as yet unpublished calculations which show the much more rapid convergence of the adiabatic dressed-state potentials using length rather than velocity gauge couplings to the excited electronic states of H_2^+, at least in the vicinity of $R \approx 2$ a.u.

[25] F. H. Mies and M. Krauss, J. Chem. Phys. **45**, 4455 (1966).

[26] M. H. Mittleman, *Theory of Laser-Atom Interactions* (Plenum, New York, 1982), p. 194.